

computational cost is lower than SCA/DCA by magnitudes due to their hundreds or thousands superconfigurations/configurations at each charge state.

II. THEORETICAL METHOD

A. Rate equations

Since the detailed description of the derivation of the rate equations in MAICRM has been presented in paper I, here only a brief outline will be given. The essential of MAICRM is using an average ion to describe the properties of all the configurations at one charge state. More specifically, for an average ion Λ_{n_e} , its occupation

number $\Omega_n^{\Lambda_{n_e}}$ is the average of the configuration's orbital occupation numbers $\{w_n^{\mathbf{K}_{n_e}}\}$ of one charge and its population $P_{\Lambda_{n_e}}$ is the summation of the configuration populations $\{P_{\mathbf{K}_{n_e}}\}$, namely

$$\begin{aligned}\Omega_n^{\Lambda_{n_e}} &= \frac{\sum_{\mathbf{K}_{n_e}} P_{\mathbf{K}_{n_e}} w_n^{\mathbf{K}_{n_e}}}{\sum_{\mathbf{K}_{n_e}} P_{\mathbf{K}_{n_e}}} \\ P_{\Lambda_{n_e}} &= \sum_{\mathbf{K}_{n_e}} P_{\mathbf{K}_{n_e}}\end{aligned}\quad (1)$$

Here \mathbf{K}_{n_e} labels a configuration of n_e bound electrons.

By summing the rate equations of orbital occupations of the configurations multiplied by the configuration population, we get the rate equations of $P_{\Lambda_{n_e}}$ and $\Omega_n^{\Lambda_{n_e}}$

$$\begin{aligned}\frac{d(P_{\Lambda_{n_e}} \Omega_n^{\Lambda_{n_e}})}{dt} &= P_{\Lambda_{n_e}} \frac{d\Omega_n^{\Lambda_{n_e}}}{dt} + \Omega_n^{\Lambda_{n_e}} \frac{dP_{\Lambda_{n_e}}}{dt} \\ &= P_{\Lambda_{n_e}} \sum_l (\mathbf{g}_n - \Omega_n^{\Lambda_{n_e}}) \Omega_l^{\Lambda_{n_e}} \mathbf{R}_{n_e, l \rightarrow n}^{\text{E/D}} - P_{\Lambda_{n_e}} \sum_l (\mathbf{g}_l - \Omega_l^{\Lambda_{n_e}}) \Omega_n^{\Lambda_{n_e}} \mathbf{R}_{n_e, n \rightarrow l}^{\text{E/D}} \\ &\quad + \Omega_n^{\Lambda_{n_e}} P_{\Lambda_{n_e+1}} \sum_i \Omega_i^{\Lambda_{n_e+1}} \mathbf{R}_{n_e+1, i \uparrow}^{\text{I}} + \Omega_n^{\Lambda_{n_e}} P_{\Lambda_{n_e-1}} \sum_i (\mathbf{g}_i - \Omega_i^{\Lambda_{n_e-1}}) \mathbf{R}_{n_e-1, i \downarrow}^{\text{R}} \\ &\quad - \Omega_n^{\Lambda_{n_e}} P_{\Lambda_{n_e}} \sum_i \Omega_i^{\Lambda_{n_e}} \mathbf{R}_{n_e, i \uparrow}^{\text{I}} - \Omega_n^{\Lambda_{n_e}} P_{\Lambda_{n_e}} \sum_i (\mathbf{g}_i - \Omega_i^{\Lambda_{n_e}}) \mathbf{R}_{n_e, i \downarrow}^{\text{R}} \\ &\quad + \Omega_n^{\Lambda_{n_e}} P_{\Lambda_{n_e+1}} \sum_{l, u, i} (\mathbf{g}_l - \Omega_l^{\Lambda_{n_e+1}}) (\Omega_u^{\Lambda_{n_e+1}} - \delta_{ui}) \Omega_i^{\Lambda_{n_e+1}} \mathbf{R}_{n_e+1, u \rightarrow l, i \uparrow}^{\text{AI}} \\ &\quad + \Omega_n^{\Lambda_{n_e}} P_{\Lambda_{n_e-1}} \sum_{l, u, i} \Omega_l^{\Lambda_{n_e-1}} (\mathbf{g}_u - \Omega_u^{\Lambda_{n_e-1}} - \delta_{ui}) (\mathbf{g}_i - \Omega_i^{\Lambda_{n_e-1}}) \mathbf{R}_{n_e-1, l \rightarrow u, i \downarrow}^{\text{EC}} \\ &\quad - \Omega_n^{\Lambda_{n_e}} P_{\Lambda_{n_e}} \sum_{l, u, i} (\mathbf{g}_l - \Omega_l^{\Lambda_{n_e}}) (\Omega_u^{\Lambda_{n_e}} - \delta_{ui}) \Omega_i^{\Lambda_{n_e}} \mathbf{R}_{n_e, u \rightarrow l, i \uparrow}^{\text{AI}} \\ &\quad - \Omega_n^{\Lambda_{n_e}} P_{\Lambda_{n_e}} \sum_{l, u, i} \Omega_l^{\Lambda_{n_e}} (\mathbf{g}_u - \Omega_u^{\Lambda_{n_e}} - \delta_{ui}) (\mathbf{g}_i - \Omega_i^{\Lambda_{n_e}}) \mathbf{R}_{n_e, l \rightarrow u, i \downarrow}^{\text{EC}}\end{aligned}\quad (2)$$

Here $\mathbf{R}^{\text{E/D}}$ are the excitation/de-excitation rate coefficients including the electron collision excitation/de-excitation and the photon excitation and spontaneous & stimulated emissions processes. $\mathbf{R}^{\text{I/R}}$ are the ionization/recombination rate coefficients including the electron collision ionization/three-body recombination and photon ionization/radiative recombination processes. $\mathbf{R}^{\text{AI/EC}}$ are the autoionization and electron capture rate equations. All the single-orbital rate coefficients are only

the functions of the charge stage, whose calculation formulas are listed in appendix A of paper I. Here is our first assumption that besides the single-orbital rate coefficients the single-orbital transition energies and oscillator strengths (without the occupation numbers) are the same for the configurations of the same charge.

Considering the bound-bound transition processes are usually faster than the bound-free atomic processes, we decouple Eq.(2) into two rate equations:

$$\frac{d\Omega_n^{\Lambda_{ne}}}{dt} = (\mathbf{g}_n - \Omega_n^{\Lambda_{ne}}) \sum_l \Omega_l^{\Lambda_{ne}} \mathbf{R}_{n_e, l \rightarrow n}^{\text{E/D}} - \Omega_n^{\Lambda_{ne}} \sum_l (\mathbf{g}_l - \Omega_l^{\Lambda_{ne}}) \mathbf{R}_{n_e, n \rightarrow l}^{\text{E/D}} \quad (3)$$

$$\begin{aligned} \frac{dP_{\Lambda_{ne}}}{dt} &= P_{\Lambda_{ne+1}} \sum_i \Omega_i^{\Lambda_{ne+1}} \mathbf{R}_{n_e+1, i \uparrow}^{\text{I}} + P_{\Lambda_{ne-1}} \sum_i (\mathbf{g}_i - \Omega_i^{\Lambda_{ne-1}}) \mathbf{R}_{n_e-1, i \downarrow}^{\text{R}} \\ &\quad - P_{\Lambda_{ne}} \sum_i \Omega_i^{\Lambda_{ne}} \mathbf{R}_{n_e, i \uparrow}^{\text{I}} - P_{\Lambda_{ne}} \sum_i (\mathbf{g}_i - \Omega_i^{\Lambda_{ne}}) \mathbf{R}_{n_e, i \downarrow}^{\text{R}} \\ &\quad + P_{\Lambda_{ne+1}} \sum_{l, u, i} (\mathbf{g}_l - \Omega_l^{\Lambda_{ne+1}}) (\Omega_u^{\Lambda_{ne+1}} - \delta_{ui}) \Omega_i^{\Lambda_{ne+1}} \mathbf{R}_{n_e+1, u \rightarrow l, i \uparrow}^{\text{AI}} \\ &\quad + P_{\Lambda_{ne-1}} \sum_{l, u, i} \Omega_l^{\Lambda_{ne-1}} (\mathbf{g}_u - \Omega_u^{\Lambda_{ne-1}} - \delta_{ui}) (\mathbf{g}_i - \Omega_i^{\Lambda_{ne-1}}) \mathbf{R}_{n_e-1, l \rightarrow u, i \downarrow}^{\text{EC}} \\ &\quad - P_{\Lambda_{ne}} \sum_{l, u, i} (\mathbf{g}_l - \Omega_l^{\Lambda_{ne}}) (\Omega_u^{\Lambda_{ne}} - \delta_{ui}) \Omega_i^{\Lambda_{ne}} \mathbf{R}_{n_e, u \rightarrow l, i \uparrow}^{\text{AI}} \\ &\quad - P_{\Lambda_{ne}} \sum_{l, u, i} \Omega_l^{\Lambda_{ne}} (\mathbf{g}_u - \Omega_u^{\Lambda_{ne}} - \delta_{ui}) (\mathbf{g}_i - \Omega_i^{\Lambda_{ne}}) \mathbf{R}_{n_e, l \rightarrow u, i \downarrow}^{\text{EC}} \end{aligned} \quad (4)$$

Eq.(3) and Eq.(4) are solved sequentially and iteratively. Firstly, we solve Eq.(3) to obtain a set of $\{\Omega_n^{\Lambda_{ne}}\}$ and then solve Eq.(4) to obtain $\{P_{\Lambda_{ne}}\}$ with the fixed $\{\Omega_n^{\Lambda_{ne}}\}$. Then the electron density N_e is updated according to the new ion populations $\{P_{\Lambda_{ne}}\}$ and all the single-orbital rate coefficients \mathbf{R} are recalculated. In succession, Eq.(3) and Eq.(4) are solved sequentially like step one. The iteration continues until N_e is invariable and the converged $\{P_{\Lambda_{ne}}\}$ and $\{\Omega_n^{\Lambda_{ne}}\}$ are obtained. During the iteration, the influence of excitation/de-excitation processes on $\{P_{\Lambda_{ne}}\}$ are implemented by $\{\Omega_n^{\Lambda_{ne}}\}$ in Eq.(4) and the influence of the ionization/recombination processes on $\{\Omega_n^{\Lambda_{ne}}\}$ are implied by the variance of N_e . The applicable conditions for decoupling Eq.(2) is that the mutual influence of $\{P_{\Lambda_{ne}}\}$ and $\{\Omega_n^{\Lambda_{ne}}\}$ is weak. In some extreme plasma conditions, the decoupling is inappropriate and should be dealt with specially. For example, in magnetic fusion, which is a very low density plasma condition, the configurations at each charge stage accumulate on the ground state and the excited orbital occupation numbers are tiny, therefore the influence of the ionization/recombination processes on the excited orbital occupations is notable which will lead to a very slow or even unsuccessful converging process for solving the rate equations.

B. Spectrum

The n th moment of the distribution for a transition array (A→B) is

$$\mu_n = \frac{\sum_{a \in A, b \in B} (E_{ab}^{\mathbf{K}_{ne}})^n \mathbf{w}_{ab}}{\mathbf{W}} \quad (5)$$

Here \mathbf{w}_{ab} , the weight of the a→b transition, is equal to the transition rate coefficient $P_{\mathbf{K}_{ne}} w_a (g_b - w_b) \mathbf{R}_{ab}$ with

g and w are the orbital statistic weight and occupation number respectively. \mathbf{R}_{ab} is the single-orbital rate coefficient. $\mathbf{W} = \sum_{a,b} \mathbf{w}_{ab}$.

The position and width of array A→B for an average ion Λ_{ne} are the first- and second-order moments respectively

$$\begin{aligned} E_{ab}^{\Lambda_{ne}} &= \mu_1 = \frac{\sum_{\mathbf{K}_{ne}} E_{ab}^{\mathbf{K}_{ne}} \mathbf{w}_{ab}}{\mathbf{W}} \\ (\Delta E_{ab}^{\Lambda_{ne}})^2 &= \mu_2 = \frac{\sum_{\mathbf{K}_{ne}} (E_{ab}^{\mathbf{K}_{ne}} - E_{ab}^{\Lambda_{ne}})^2 \mathbf{w}_{ab}}{\mathbf{W}} \end{aligned} \quad (6)$$

Here $\sum_{a,b}$ is replaced by $\sum_{\mathbf{K}_{ne}}$ since the array for an average ion includes all the configurations of the same number of bound electrons, i.e., \mathbf{n}_e .

The zero- and first-order configuration-average energies are[4]

$$\begin{aligned} E^{\mathbf{K}_{ne}(0)} &= \sum_s w_s \varepsilon_s \\ E^{\mathbf{K}_{ne}(1)} &= \sum_s w_s \langle s \rangle + \frac{1}{2} \sum_{r,s} w_s (w_r - \delta_{rs}) \langle r, s \rangle \end{aligned}$$

Here w_s and ε_s are the orbital occupation number and orbital energy. $\langle s \rangle$ and $\langle r, s \rangle$ are respectively the one- and two-electron matrix elements shown in Appendix B of Ref.[4].

The zero- and first-order configuration-average transition energies for a→b transition are

$$\begin{aligned} E_{ab}^{\mathbf{K}_{ne}(0)} &= \varepsilon_b - \varepsilon_a \\ E_{ab}^{\mathbf{K}_{ne}(1)} &= D_0 + \sum_s (w_s - \delta_{sa}) D_s \end{aligned}$$

Here $D_0 = \langle b \rangle - \langle a \rangle$ and $D_s = \langle s, b \rangle - \langle s, a \rangle$.

If we put $E_{ab}^{\mathbf{K}_{ne}(0)}$ into Eq.(6), we get $E_{ab}^{\Lambda_{ne}(0)} = \varepsilon_b - \varepsilon_a$ and $(\Delta E_{ab}^{\Lambda_{ne}(0)})^2 = 0$.

In the present work, we use the following formulas to calculate the position and width of the array, which are derived from formulas (35) and (36) of Ref.[4] by using

$$E_{ab}^{\Lambda_{ne}(1)} = D_0 + \sum_s \frac{\Omega_s^{\Lambda_{ne}}}{g_s} g_s^{ab} D_s$$

$$(\Delta E_{ab}^{\Lambda_{ne}(1)})^2 = \sum_{t,r} \left(\frac{\Omega_t^{\Lambda_{ne}}}{g_t} g_t^{ab} D_t \right) \left(\frac{\Omega_r^{\Lambda_{ne}}}{g_r} g_r^{ab} D_r \right) + \sum_t \frac{\Omega_t^{\Lambda_{ne}}}{g_t} g_t^{ab} D_t^2 - (E_{ab}^{\Lambda_{ne}(1)} - D_0)^2 \quad (7)$$

Here $g_t^{ab} = g_t - \delta_{at} - \delta_{bt}$ and $g_r^{abt} = g_r - \delta_{ar} - \delta_{br} - \delta_{tr}$.

Comparatively, in AA model, the summation of the orbital rate equations are carried out on all the configurations at all ionic stages and the position and width of the transition array are

$$E_{ab}^{(AA)} = D_0 + \sum_s \mathbf{p}_s g_s^{ab} D_s$$

$$(\Delta E_{ab}^{(AA)})^2 = \sum_t \mathbf{p}_t (1 - \mathbf{p}_t) g_t^{ab} D_t^2 \quad (8)$$

Here \mathbf{p}_s is the occupation probability of orbital s , i.e., the ratio of the orbital occupation number to the statistic weight.

III. RESULTS AND DISCUSSIONS

In this work, 65 single orbital bases nlj ($n \leq 5$) and nl ($5 < n \leq 10$) are used (listed in paper I).

Fig.1 shows the comparisons of the one-electron transition emission spectra for Fe plasma at $T=200\text{eV}$, $N_i = 8.5 \times 10^{22} \text{ cm}^{-3}$ and Pr plasma at $T=250\text{eV}$, $N_i = 10^{20} \text{ cm}^{-3}$. The emissive intensity of Ref.[4] is in arbitrary units. As shown in Fig.1, compared with the STA curves, which are of a single supershell for each charge state, the widths of MAICRM curves are in good agreement, while the line positions show about 2% red shifts, namely about 11eV for Fe and about 0.2Å for Pr. The shifts of the positions should result from the difference of the ionization distribution and the atomic data including the orbital energies and transition matrix elements. The widths of the AA curves are obviously broader than MAICRM and STA. From the statistic angle, the spectra of MAICRM and STA with a single supershell are both the function of the average orbital occupations of the configurations at one charge stage while the average orbital occupations are determined by different ways, namely by solving the excitation/de-excitation rate equations for MAICRM and by assuming a Boltzmann distribution for STA.

Fig.2 shows the comparison of the emissivity of Xe plasma at $T_e=4\text{keV}$ and $N_e = 3.6 \times 10^{20} \text{ cm}^{-3}$. The detailed gray curve is calculated by SCRAM codes which uses hybrid atomic data, including levels, configurations

the first-order configuration energy $E_{ab}^{\mathbf{K}_{ne}(1)}$.

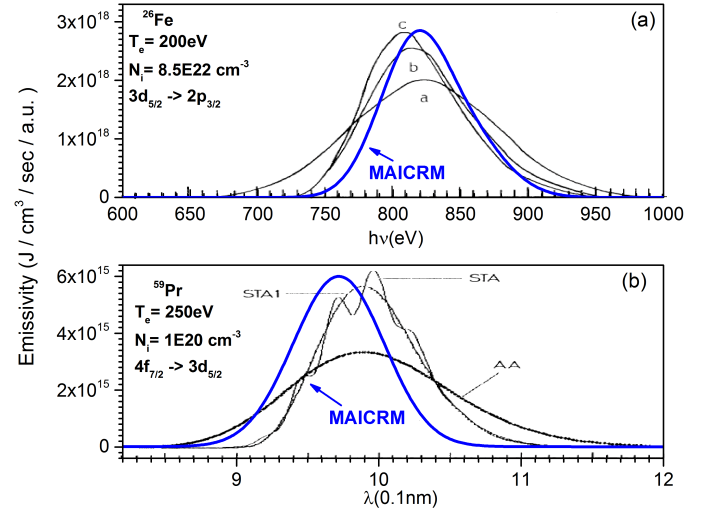


FIG. 1. (Color online) The comparisons of the one-electron transition emission spectra for Fe and Pr plasmas. The emissive intensity from Ref.[4] is in arbitrary units. (a) Emission spectra for the one-electron transition $3d_{5/2} - 2p_{3/2}$ of Fe plasma at $T = 200\text{eV}$ and $N_i = 8.5 \times 10^{22} \text{ cm}^{-3}$. Curve a : AA result (zeroth-order energies); curve b : STA result with a single supershell for each charge state and zeroth-order energies; and curve c : STA result with a single supershell for each charge state but using first-order energies. (b) Emission spectra for the one-electron transition $4f_{7/2} - 3d_{5/2}$ of Pr plasma at $T = 250\text{eV}$ and $N_i = 10^{20} \text{ cm}^{-3}$. Curve of AA : AA method; curve of STA : convergence with increasing number of STA; curve of STA1 : single supershell for each charge state.

and superconfigurations, constructed from a combination of fine structure and unresolved transition array (UTA) data from FAC, supplemented with the extended screened-hydrogenic model (including satellite shifts)[11]. The red curve is calculated by extended 'DCA' codes which construct atomic levels as superconfigurations or Layzer complexes by shells described by principal quantum numbers with two extensions: one is to split each photoexcitation transition between principal quantum numbers into multiple term-to-term transitions with in-

dividual energies and oscillator strengths; the other one is to assign an additional width to each transition, representing additional unresolved fine structure multiplets, modeling each transition as an UTA[7]. Here SCRAM and 'DCA' use a set of similar superconfigurations for each ionic stage, thus their calculated average ionizations $\langle Z \rangle_{\text{SCRAM}} = 42.9$ and $\langle Z \rangle_{\text{'DCA'}} = 43.0$ agree well. $\langle Z \rangle_{\text{MAICRM}} = 43.4$ is higher by about 0.5.

In Fig.2 the mean features of the three curves are in general agreement although MAICRM and extended 'DCA' have no the fine structures of SCRAM. Compared to the detailed gray spectrum of SCRAM, MAICRM curve agrees better than 'DCA' curve at some places such as the peaks at 310eV and the relative intensities of three peaks at 155eV, 190eV and 220eV. The peak of MAICRM curve at 105eV is closer to the maximum position of gray curve than the red curve. The continue background of MAICRM at energies larger than 1keV is lower than the grey and red curves which should result from the difference of $\langle Z \rangle$.

Fig.3 shows the comparison of the emissivity of Au plasma at $T_e=1\text{keV}$, $T_r=400\text{eV}$ and $\rho=0.0155\text{g/cm}^3$. Here DCA is the traditional detailed configuration accounting model, RDCA is a reduced DCA model and XSN is a AA model[7]. RDCA model makes an average of the energies and cross-sections of the detailed states falling within a spectral energy grid divided according to the DCA energy level structure of an ion[7]. Compared with $\langle Z \rangle_{\text{DCA}}=51.8$, $\langle Z \rangle_{\text{MAICRM}}=52.6$ is much closer than $\langle Z \rangle_{\text{XSN}}=56.5$. For clarity, the blue curve of MAICRM is added into the three panels. Panel (a) shows the MAICRM curve agrees well with the DCA curve especially at energies larger than 1keV. In the energy range of 80eV-120eV, the widths of MAICRM curve are larger than DCA. Panel (b) shows the RDCA curve differs from the MAICRM curve in many places. In panel (c) the XSN curve shows simpler structure and broader peaks than MAICRM since in AA model only one average ion is considered.

IV. CONCLUSION

We have developed a general model to simulate the plasma properties of hot dense plasma. The average orbital occupations and total population for the configurations within one charge state are characterized by an average ion. The orbital occupation $\{\Omega_n^{\Lambda_{n_e}}\}$ and population $\{P_{\Lambda_{n_e}}\}$ of the average ion Λ_{n_e} are obtained by solving two sets of rate equations sequentially and iteratively. Our calculated CSDs as well as the spectra of hot dense plasmas agree with DCA/SCA models as shown in paper I and this work. On the other hand, since MAICRM only considers one configuration at each charge state the computational cost reduces magnitudes compared to DCA/SCA models due to their hundreds or thousands atomic levels at one charge state, which means

the possibility to be coupled into radiation-transport hy-

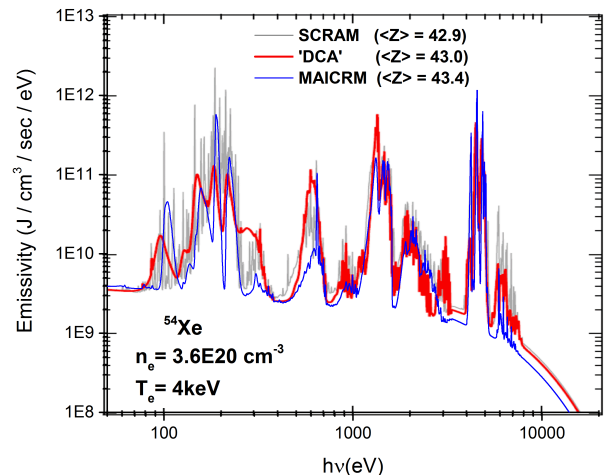


FIG. 2. (Color online) The calculated emissivity as a function of photon energy for Xe plasma at $T_e=4\text{keV}$ and $N_e = 3.6 \times 10^{20} \text{ cm}^{-3}$. The results of 'DCA' and SCRAM are from Ref.[7].

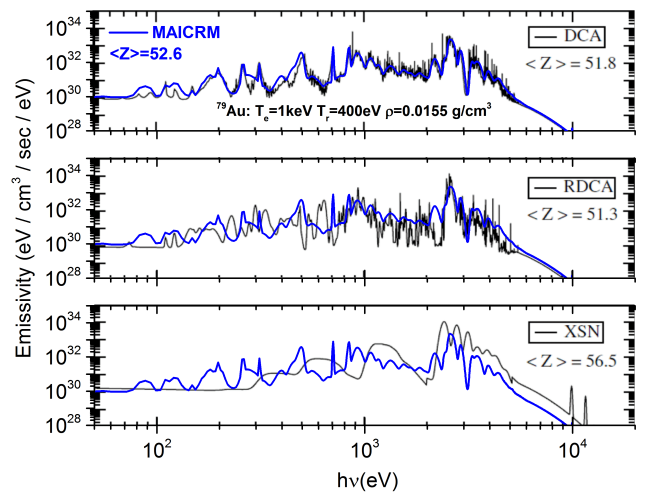


FIG. 3. (Color online) The calculated emissivity as a function of photon energy for Au plasma at $T_e=1\text{keV}$, $T_r=400\text{eV}$ and a mass density of 0.0155 g/cm^3 . For clear comparison with the results of DCA, RDCA and XSN of Ref.[6], the blue curve of MAICRM is added into the three panels.

drodynamic simulations in the future.

ACKNOWLEDGMENTS

This work is partly supported by the National Key R&D Program of China Under Grant No. 2017YFA0402300.

-
- [1] D. R. Bates, A. E. Kingston and R. W. P. McWhirter, Proc. R. Soc. A **267**, 297 (1962).
- [2] Yuri Ralchenko, Modern methods in collisional-radiative modeling of plasmas (Springer Series on Atomic, Optical, and Plasma Physics, 2016)
- [3] J. Bauche, C. Bauche-Arnoult, and M. Klapisch, J. Phys. B **24**, 1 (1991).
- [4] A. Bar-Shalom, J. Oreg, W. H. Goldstein, D. Shvarts, and A. Zigler, Phys. Rev. A **40**, 3183 (1989).
- [5] Joseph Abdallah Jr and M. E. Sherrill, High Energy Density Phys. **4**, 124 (2008).
- [6] Joseph Abdallah Jr, M. E. Sherrill, D. P. Kilcrease, C. J. Fontes, H. L. Zhang and J. Oelgoetz, High Energy Density Phys. **5**, 204 (2009).
- [7] H. A. Scott and S. B. Hansen, High Energy Density Phys. **6**, 39 (2010).
- [8] X. Y. Han, L. X. Li, Z. S. Dai, W. D. Zheng, P. J. Gu and Z. Q. Wu, submitted to Acta Physica Sinica (in Chinese).
- [9] Shuji Kiyokawa, High Energy Density Phys. **13**, 40 (2014).
- [10] M. Itoh, T. Yabe and S. Kiyokawa, Phys. Rev. A **35**, 233 (1987).
- [11] S. S. B. Hansen, J. Bauche, C. Bauche-Arnoult, and M. F. Gu, High Energy Density Phys. **3**, 109 (2007).